Climate Dynamics (2018) 51:2681–2694
https://doi.org/10.1007/s00382-017-4036-8

Impact of chlorophyll bias on the tropical Pacific mean climate in an earth system model

Hyung-Gyu Lim[1] · Jong-Yeon Park[2,3] · Jong-Seong Kug[1]

Received: 11 April 2017 / Accepted: 5 December 2017 / Published online: 9 December 2017
© Springer-Verlag GmbH Germany, part of Springer Nature 2017

Abstract
Climate modeling groups nowadays develop earth system models (ESMs) by incorporating biogeochemical processes in their climate models. The ESMs, however, often show substantial bias in simulated marine biogeochemistry which can potentially introduce an undesirable bias in physical ocean fields through biogeophysical interactions. This study examines how and how much the chlorophyll bias in a state-of-the-art ESM affects the mean and seasonal cycle of tropical Pacific sea-surface temperature (SST). The ESM used in the present study shows a sizeable positive bias in the simulated tropical chlorophyll. We found that the correction of the chlorophyll bias can reduce the ESM's intrinsic cold SST mean bias in the equatorial Pacific. The biologically-induced cold SST bias is strongly affected by seasonally-dependent air–sea coupling strength. In addition, the correction of chlorophyll bias can improve the annual cycle of SST by up to 25%. This result suggests a possible modeling approach in understanding the two-way interactions between physical and chlorophyll biases by biogeophysical effects.

Keywords Phytoplankton · Climate model bias · Biogeochemical model · Biogeophysical feedback · GFDL-ESM · Air–sea coupling · CMIP5

1 Introduction

Phytoplankton are single-celled organisms at the base of the pelagic food web; they contribute to global biogeochemical (BGC) processes. The dynamics of phytoplankton growth (Geider et al. 1997) and BGC particle exports (Dunne et al. 2005, 2007) have been formulated in several BGC models to consider BGC processes (Oka et al. 2009; Dunne et al. 2013; Azhar et al. 2014; Stock et al. 2014). The earth system model (ESM), a climate model embedded with BGC model, can now advance understanding of climate feedbacks associated with global carbon flux and BGC cycle. Accordingly, ESMs participated in the fifth phase of the Coupled Model Intercomparison Project (CMIP5) have been evaluated to see the inter-model range of simulated ocean BGC properties (Taylor et al. 2012). The spatial correlation skills of present-day global patterns of simulated chlorophyll climatology against Sea-viewing Wide Field-of-view Sensor (SeaWiFS) satellite data (McClain 1998) are mostly in the range of 0.50–0.72, and those of nitrate climatology against World Ocean Atlas 2013 data (Garcia et al. 2014) are mostly in the range of 0.62–0.85, with the general agreement on the open ocean BGC patterns across the models (Laufkötter et al. 2015). Particularly, the present-day surface chlorophyll in individual ESMs captures well the observed large-scale pattern, i.e. high chlorophyll in the tropics and low chlorophyll in the subtropics (Collins et al. 2011; Watanabe et al. 2011; Buitenhuis et al. 2013; Dunne et al. 2013; Moore et al. 2013; Séférian et al. 2013).

Despite the overall good performance of CMIP5 ESMs, they still have shown the considerable mean bias and inter-model diversity of marine BGC variables, such as chlorophyll concentration, nutrients, net primary production

✉ Jong-Yeon Park
jongyeon@princeton.edu

✉ Jong-Seong Kug
jskug1@gmail.com

[1] Division of Environmental Science and Engineering, Pohang University of Science and Technology (POSTECH), 77 Cheongam-Ro Nam-Gu, Pohang 790-784, South Korea

[2] Atmospheric and Oceanic Sciences Program, Princeton University, 201 Forrestal Rd, Princeton, NJ 08540, USA

[3] National Oceanic and Atmospheric Administration/Geophysical Fluid Dynamics Laboratory, Princeton, NJ, USA

(Laufkötter et al. 2015), ocean primary production (Anav et al. 2013), and oxygen (Séférian et al. 2016). The chlorophyll bias, for example, is affected by biases in physical and BGC fields such as inconsistent strategies of spin up ESM (Séférian et al. 2016), mixed layer depth bias (Popova et al. 2012; Anav et al. 2013; Sallée et al. 2013), and nutrients (Vancoppenolle et al. 2013). In the tropical Pacific, biases of sub-surface chlorophyll maximum depth, nutrient concentrations, ocean dynamics of equatorial and coastal upwelling can also induce the chlorophyll bias (Aumont and Bopp 2006; Collins et al. 2011; Watanabe et al. 2011; Buitenhuis et al. 2013; Dunne et al. 2013; Moore et al. 2013). These results suggest that multiple combinations of model diversities in physical climate and biogeochemical conditions can cause the large uncertainty in simulated chlorophyll concentrations.

While the physical climate bias partly induces the chlorophyll bias, the biological bias may inversely affect the physical climate by changing the penetration depth of solar radiation in the ocean. Phytoplankton modulates ocean optical properties such as the shortwave attenuation by changing the inherent absorption and scattering shortwave radiation (Morel 1988; Morel and Antoine 1994; Manizza et al. 2005). The changes in chlorophyll concentration modify the upper ocean temperature by changing the biologically-induced absorption of solar radiation (Nakamoto et al. 2001; Manizza et al. 2005; Marzeion et al. 2005; Lengaigne et al. 2007; Anderson et al. 2009; Gnanadesikan and Anderson 2009; Löptien et al. 2009; Jochum et al. 2010; Lin et al. 2011; Park et al. 2014a, b). Thus, the chlorophyll concentration in marine algae is linked not only with marine primary production but also with biological and physical coupling processes that may change physical climate systems.

The current CMIP5 ESMs (e.g. CESM1, MIROC5, GFDL-ESM2M, GFDL-ESM2G, and HadGEM2-ES) have generally overestimated the chlorophyll concentration in the tropical Pacific (Collins et al. 2011; Watanabe et al. 2011; Dunne et al. 2013; Moore et al. 2013). Given that many ESMs consider chlorophyll-based shortwave penetration schemes, most of which are based on a chlorophyll-based parameterization of Morel (1988) and Lambert–Beer's law, the reported chlorophyll bias in ESMs can induce an undesirable physical bias in the ocean. GFDL-ESM, the model used in the present study, is also suffering from the overestimated chlorophyll bias in the tropical Pacific (Dunne et al. 2013), which may contribute to the equatorial cold sea-surface temperature (SST) bias in GFDL-ESM.

The mechanisms of the biologically-driven cold SST response in Modular Ocean model (MOM) based GFDL model simulation is explained by "biogeophysical" (or so-called bio-optical, biophysical) effect (Manizza et al. 2005; Gnanadesikan and Anderson 2009; Löptien et al. 2009; Park et al. 2014a, b). (1) The higher chlorophyll concentration in the equatorial Pacific absorbs more shortwave radiation in the upper layer of ocean and less shortwave radiation in the subsurface layer by so-called "self-shading effect". This redistribution of vertical shortwave heating enhances oceanic stratification. (2) Ocean mixed layer becomes shallower due to the relatively stabilized ocean. (3) The shallower mixed layer can lead to strong Ekman divergence even with the same magnitude of easterly wind stress forcing along the equator (Sweeney et al. 2005). The enhanced Ekman transport toward the off-equator induces the meridional mass transport. (4) To satisfy the mass conservation, oceanic upwelling along the equator is enhanced. Consequently, the ocean surface becomes cooler than the case with lower chlorophyll concentration. In a fully-coupled atmosphere–ocean–BGC modeling study, the biologically-induced SST cooling is further intensified by the atmospheric response associated with the Bjerknes feedback (Bjerknes 1968; Park et al. 2014b).

The physical component of GFDL-ESM has reported the intrinsic cold SST bias due to equatorial physical biases such as the strong zonal wind and the shallow thermocline depth (Delworth et al. 2006; Wittenberg et al. 2006). The physical bias of strong zonal wind may enhance the replenishment of nutrients leading to the overestimated chlorophyll in the ESM. This overestimated chlorophyll can also intensify the cold SST in the equatorial Pacific by the biogeophysical effect as mentioned above. In other words, physical biases in a model, which is previously unresolved, can lead to an additional biological bias despite the progress in earth system modeling. Thus, the mean state in an ESM can be affected by two-way interactions between physical and BGC biases. While there have been great efforts to investigate and quantify the impact of biogeophysical feedbacks on the mean state and seasonal cycle of SST (Manizza et al. 2005; Lengaigne et al. 2007; Mignot et al. 2013; Park et al. 2014a, b), little effort has been made to quantify how much the systematic biases in BGC fields affect the mean bias of physical variables in a coupled climate system.

The purpose of the present study is to examine how and how much the chlorophyll bias can affect physical systems in the tropical Pacific. We conduct idealized model experiments using a GFDL's earth system model that has a similar model configuration with GFDL-ESM2M in CMIP5 (Dunne et al. 2013). Section 2 shows the detailed description of observational data and model experiments. Results are presented in Sect. 3: Sect. 3.1 shows the chlorophyll bias of model experiments. Section 3.2 shows the biogeophysical impact of chlorophyll bias on annual mean SSTs. Section 3.3 describes the seasonal dependency of biologically-induced climate responses. Section 3.4 shows the annual cycle of SST responses. Finally, Sect. 4 presents summary and discussion.

2 Description of observations and models

2.1 Observational data

Observational chlorophyll concentration used in this study is the satellite-retrieved data from Sea-viewing Wide Field-of-view Sensor (SeaWiFS; McClain 1998) and Moderate Resolution Imaging Spectroradiometer (MODIS; Esaias et al. 1998) provided from Goddard Space Flight Center (http://oceancolor.gsfc.nasa.gov). These two data sets cover the concentration of chlorophyll-a spanning from September 1997 to the present time. Those records are aggregated together using the SeaWiFS data from January 1998 to December 2002 and the MODIS data from January 2003 to December 2014. The ocean surface chlorophyll data are monthly level-3 products binned to a horizontal grid of 9 km. In this study, the data are bilinearly interpolated to a 1.0° × 1.0° grid for computational efficiency and for comparison with simulated chlorophyll from the earth system model we used.

Observational SST data used to evaluate the SST bias of the model are from the Extended Reconstructed SST version 3 (ERSST v3) derived from *in situ* measurements, with a spatial resolution of 2.0° × 2.0°. (Smi et al. 2008). Observational zonal momentum flux (zonal wind stress) used in this study is obtained from the National Centers for Environmental Prediction–National Center for Atmospheric Research (NCEP–NCAR) reanalysis 1 dataset over the recent six decades (Kalnay et al. 1996).

2.2 Numerical model

We employ the global coupled atmosphere–ocean–ice–land–BGC model developed by Geophysical Fluid Dynamics Laboratory (GFDL). All models are from community codes of GFDL (https://www.gfdl.noaa.gov/earth-system-model/). This earth system model (ESM) consists of an Atmospheric Model (AM2), a Land Model (LM2), a Sea Ice Simulator (SIS), a new generation of Modular Ocean Model version 5 (i.e. MOM5), and a BGC model named as Tracers of Phytoplankton with Allometric Zooplankton version 2 (TOPAZv2) (Dunne et al. 2012, 2013).

The AM2 has horizontal resolution 2° latitude × 2.5° longitude on a regular grid and 24 vertical levels in a hybrid coordinate system. The dynamical core of AM2 uses the finite volume method (Anderson et al. 2004; Lin 2004). The LM2 has the same horizontal resolution as AM2 (i.e., 2° latitude × 2.5° longitude on a regular grid) and includes soil, sensible and latent heat storage, groundwater storage, and stomatal resistance (Anderson et al. 2004). The SIS incorporates full ice dynamics, three-layer framework, five different ice thickness categories, and the same tripolar grid on the open ocean similar to the ocean component of the model (Murray 1996; Winton 2000). For the MOM5 (Griffies 2012), the resolution is a 1° in latitude and longitude between 30° and 65°, telescopes to 1/3° toward the equatorial region. The grid spacing of MOM5 in the polar region is non-uniform; the horizontal grid switches from spherical to bipolar poleward from 65° (Murray 1996). The MOM5 has a C-grid layout option for the horizontal gridding of the discrete model fields to develop fine-resolution experiment and to solve a coupled set of Eulerian and Lagrangian equations that is interacting through the exchange of mass, tracers, and momentum. The BGC model, named TOPAZv2, considers 30 tracers including the chlorophyll concentration, cycles of carbon, nitrogen, phosphorus, silicon, iron, oxygen, alkalinity, lithogenic material, calcite, aragonite, and detritus (Dunne et al. 2013).

The penetrative shortwave heating of the present model experiment is implemented based on the Manizza optics scheme (Manizza et al. 2005). The fraction of total surface irradiance between infrared and visible wavelength bands is determined by surface condition in atmospheric model. The infrared of total surface irradiance is absorbed within 2-m of the ocean about 99.9% (Morel and Antoine 1994). In contrast, the visible bands of shortwave solar radiation, partitioned between red and blue/green, transfer the ocean column down to the cutoff depth (200-m in this study). In this case, attenuation coefficients are determined by diagnosed vertical profile of chlorophyll concentration simulated from the bio-geochemical model. This optics scheme considers self-shading effects. That is, the shortwave heating of the deeper ocean layer is affected by chlorophyll precondition of the upper layer that absorbs shortwave radiation first. This scheme allows to compute the biogeophysical feedback processes in every integration time in global scales.

2.3 Experimental design

Three experimental sets are conducted (Table 1): OGCM, ESM_on, and ESM_off. OGCM, and ESM_on are the experiments with the BGC model switched on, but ESM_off is the experiment with the BGC model switched off. In all experimental sets, the Manizza et al. (2005) biogeophysical scheme is used.

First, in the OGCM (i.e., MOM5, SIS) experiment, the TOPAZv2 model simulates three-dimensional chlorophyll concentration. In these experiments, historical observed 6-h zonal and meridional winds from January 1951 to December 2014 are prescribed and three ensemble members are integrated from different initial condition. The historical observed wind forcing is obtained from the NCEP/NCAR

Table 1 Summary of experiments

Exp.	Model	Biological component	Simulated period
OGCM	MOM5 + TOPAZv2	Simulated chlorophyll	64 years × 3 after 600 year spin-up
ESM_on	CM2.1 + TOPAZv2	Simulated chlorophyll	100 years after 600 year spin-up
ESM_off	CM2.1	Prescribed chlorophyll from OGCM into tropical Pacific and from ESM_on into the other region	200 years × 3 after 700 year spinup

reanalysis I (Kalnay et al. 1996). To avoid a long-term drift, ocean initial conditions are obtained after more than 600-year spin-up period. Other boundary conditions, such as shortwave radiation, longwave radiation, near-surface specific humidity, precipitation, and air temperature are from the Common Ocean–Ice Reference Experiment (CORE; Large and Yeager 2004).

In the second experiment, ESM_on, the GFDL-CM2.1 (i.e., MOM5, SIS, AM2, and LM2) coupled with the TOPAZv2 is used. After a 300-yr spinup in the ocean-only model experiment (i.e. OGCM), another 400-year-long run is performed with the fully coupled model (CM2.1), and then the last 100-year is analyzed.

In the third experiment, ESM_off, the same model configuration as in ESM_on is used but with switching off the TOPAZv2. Instead, climatological monthly mean of chlorophyll concentration in OGCM and ESM_on is prescribed: In the tropical Pacific (120°E–70°W, 20°N–20°S), the 3-dimensional climatological monthly mean of the chlorophyll simulated in OGCM (1998–2014) is prescribed. In the region outside the tropical Pacific, the climatological mean of chlorophyll simulated in ESM_on is prescribed. The idea behind this experimental design is that the chlorophyll bias in ESM_on is reduced by prescribing the tropical chlorophyll concentration simulated by OGCM that simulates a more comparable chlorophyll to the satellite chlorophyll than ESM_on (see Figs. 1, 2). The reasoning behind this experimental design is that directly prescribing satellite chlorophyll may not be a proper way to isolate the SST bias driven by chlorophyll bias given that the vertical structure of chlorophyll is acknowledged to play an important role in the response of SST to biogeophysical feedback (e.g. Lengaigne et al. 2007). Three ensemble members are integrated with different initial conditions. ESM_off is integrated for 200-year and the ensemble mean of the last 150-year is used for the comparison with results of ESM_on. The results shown in the present study are not much sensitive to the choice of integration period.

The external forcings, preindustrial atmospheric nitrogen deposition (Horowitz et al. 2003), preindustrial runoff nitrogen flux (Green et al. 2004), preindustrial lithogenic dust and soluble iron (Fan et al. 2006), are prescribed into TOPAZv2 of OGCM and ESM_on experiments. For the comparison with observation in horizontal field, the simulated

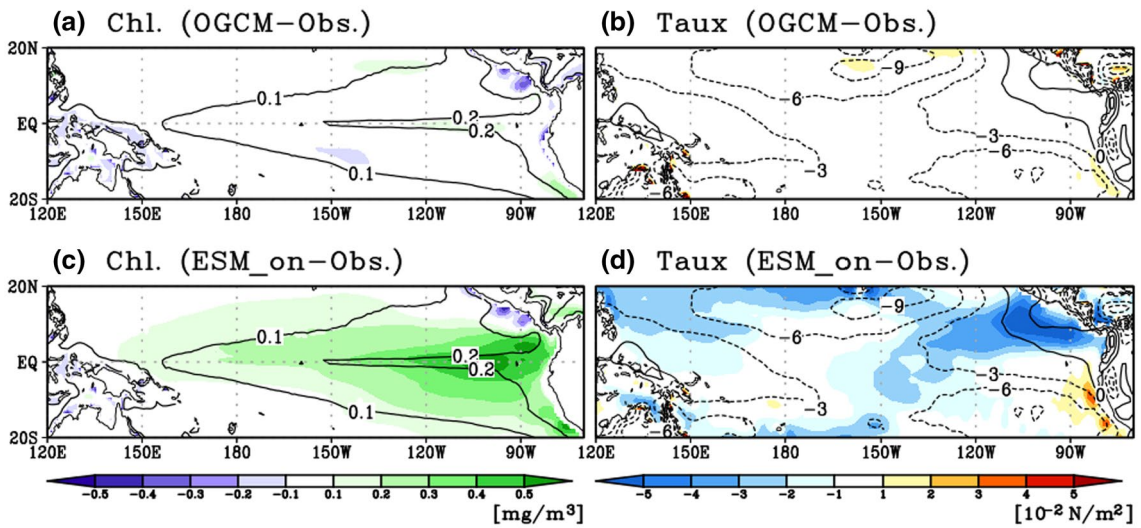

Fig. 1 Upper panels are the observational annual mean (contour) and annual mean difference (shade) of **a** chlorophyll concentration and **b** zonal wind stress between OGCM and observation. Bottom panels (**c, d**) are the same as upper panels (**a, b**), except for the difference between ESM_on and observation. The annual means of OGCM and observation are averaged from January 1998 to December 2014, the annual mean of ESM_on is averaged 100 years

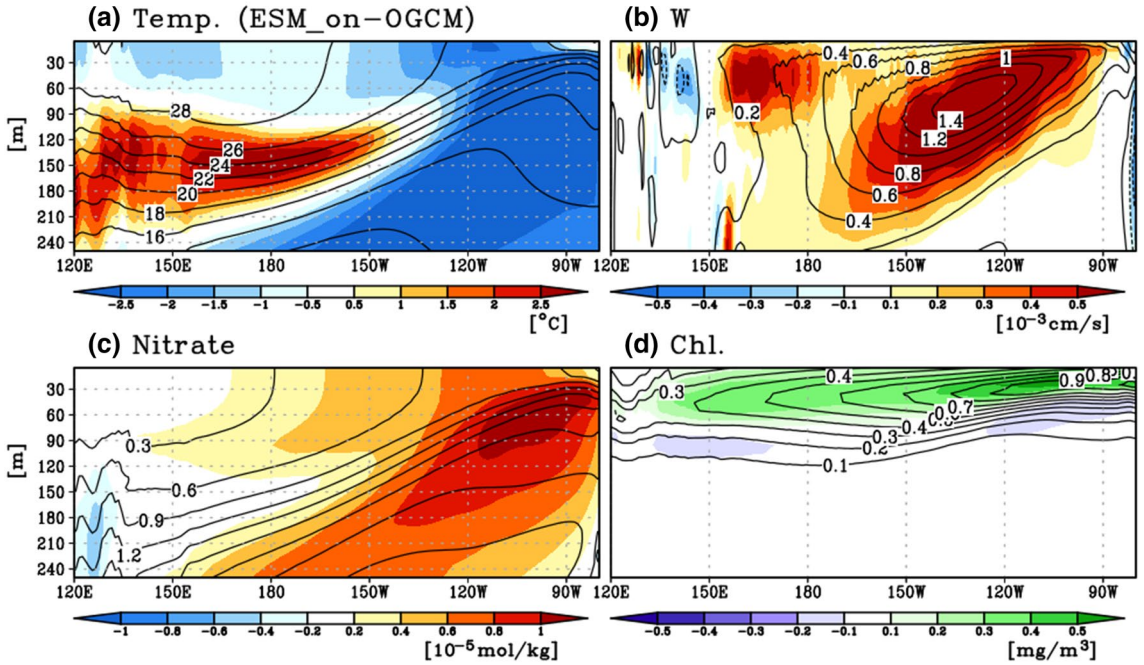

Fig. 2 The vertical section above 250 m of **a** the climatological mean temperature of ESM_on (contour) and the mean difference of temperature (shade) between ESM_on and OGCM along the equator (5°N–5°S). **b** is the same as **a**, except for the vertical velocity averaged in 2°N:2°S. **c, d** are the same as **a**, except for nitrate and chlorophyll

chlorophyll in our study is averaged over the upper 20 m, given that the satellite-retrieved ocean color data is based on light reflected primarily from the upper ocean layer including a backscatter within the mixed layer.

3 Results

3.1 Chlorophyll biases in OGCM and ESM_on

Prior to examining the impact of chlorophyll bias, we firstly check how well OGCM and ESM_on simulate the observed climatological distribution of chlorophyll concentration. In the tropical Pacific, the climatological mean of the observational chlorophyll shows permanently high-east and low-west patterns (contours in Fig. 1a). Strong equatorial upwelling, which carries nutrients from the subsurface to the surface water, leads to phytoplankton growth over the eastern Pacific because the tropical Pacific is a well-known nutrient limitation region (Chavez et al. 1999). The simulated climatology of chlorophyll concentration obtained from OGCM is mostly similar with the observed chlorophyll concentration (Fig. 1a). In addition to the climatology, OGCM simulates well the interannual variability of chlorophyll concentration over the tropical Pacific. The correlation coefficient between the observed and simulated chlorophyll concentrations during 1998–2014 is about 0.6 in the tropical Pacific (120°E–70°W, 20°N–20°S). Particularly, the correlation coefficient is much higher (i.e. 0.76) in the central Pacific region (160E–150W, 5S–5N). This result, which is consistent with an ocean-only modeling study (Park et al. 2014a), suggests that the observed winds exert influence on simulating chlorophyll concentration and play a major role in driving interannual chlorophyll variations.

In contrast to the OGCM experiment, the ESM_on experiment shows the excessive chlorophyll concentration over the tropical Pacific (Fig. 1c). The ocean and biogeochemical components in the two experiments, OGCM and ESM_on, are identical except atmospheric coupling, thus the strong positive bias of chlorophyll is likely related to the bias in atmospheric winds. The zonal wind stress simulated in ESM_on is zonally broader, stronger, and extending too far west than the reanalysis data over the eastern Pacific (Fig. 1d). This is consistent with a previous study (Wittenberg et al. 2006), showing the linkage between easterly wind bias and intrinsic zonal SST gradient bias along the equator. In the ESM, this stronger easterly wind stress is not only associated with the cold SST bias, but also with the enhanced phytoplankton bloom by anomalous upwelling. The high chlorophyll concentration can be advected to the central Pacific following the equatorial surface current, which contributes to the positive chlorophyll bias over the central Pacific (Fig. 1c). This implies that the mean bias of chlorophyll concentration is attributable to the bias of physical components in the ESM.

It has been reported that GFDL CM2.1, a previous version of GFDL's climate model, has intrinsic physical biases such as the strong zonal wind and the shallow thermocline depth (Delworth et al. 2006; Wittenberg et al. 2006). In this regard, the physical bias found in the ESM we used, which is previously unresolved, may cause an additional biogeochemical bias. Enhanced vertical motion induced by the strong zonal wind in the ESM would induce overestimated biogeochemical replenishment. To examine the impact of easterly wind bias on the ocean, mean differences of temperature, vertical velocity, nitrate, and chlorophyll between ESM_on and OGCM are analyzed along the equatorial upper-ocean (Fig. 2). The mean difference of the equatorial temperature shows a cooling in the eastern Pacific, indicating the shoaling of thermocline (Fig. 2a). The relatively strong easterly wind stress (Fig. 1d) can induce the excessive meridional Ekman mass transport (Sweeney et al. 2005; Park et al. 2014a). To compensate the water mass in the ocean surface, vertical velocity is increased (Fig. 2b). Consequently, the nutricline, a representative of nutrients, is shallowed by the enhanced vertical motion, leading to the increased nutrient replenishment into the mixed layer (Fig. 2c). The enriched nutrient of euphotic zone finally fuels phytoplankton blooms and the chlorophyll concentration becomes higher in the mixed layer (Fig. 2d). This result suggests that the overestimated chlorophyll concentration in ESM_on is mainly due to the strong easterly wind and the corresponding upwelling increase. In the meanwhile, the chlorophyll bias may give a biogeophysical feedback as suggested previous studies, which causes a bias of physical components.

3.2 Biogeophysical impact of chlorophyll bias on annual mean state

To examine the impact of chlorophyll bias on physical states, the ESM_off experiment is conducted by prescribing OGCM chlorophyll in the tropical Pacific. In ESM_off, the overestimated tropical Pacific chlorophyll concentration is replaced by the OGCM chlorophyll concentration that is more similar to the observed chlorophyll concentration than ESM_on. Note that the observed chlorophyll concentration cannot be directly prescribed in ESM_off simulation because the observation does not provide 3-dimensional distribution including depth. It can be anticipated that, compared to ESM_on, the corrected chlorophyll concentration in ESM_off reduces the biogeophysical absorption of shortwave radiation in the upper ocean and consequently reduces oceanic stratification. The reduced oceanic stratification in ESM_off can lead to a weaker Ekman divergence by the easterly wind stress forcing and induce a surface warming due to the reduced upwelling in the eastern Pacific as explained by previous studies (Manizza et al. 2005; Sweeney et al. 2005; Park et al. 2014a). Therefore, the correction of chlorophyll concentration may contribute to reducing intrinsic cold SST bias through the warming impact of reduced chlorophyll.

Figure 3a, b show the chlorophyll differences between ESM_on and ESM_off and between ESM_on and observation. The similar pattern and magnitude between the two figures indicates that the chlorophyll bias in ESM_on is successfully reduced in ESM_off. Given the only difference between ESM_on and ESM_off is the bias correction of chlorophyll, thus the major difference of physical fields between the two experiments can be explained by the impact of chlorophyll bias in ESM_on. Near the western coast of America, the model is still limited to simulate the realistic chlorophyll concentration because the horizontal resolution of the model is not sufficient to resolve the coastal upwelling, which can reduce chlorophyll bloom near the coastal line (Dunne et al. 2013).

The ESM_off run simulates significantly colder SSTs in the equatorial Pacific compared to ESM_on (Fig. 3c). Given the cold SST bias in ESM_on as shown in Fig. 3d, this result indicates that the chlorophyll bias in ESM_on can considerably contribute to the cold SST bias in the equatorial Pacific. In other words, the correction of chlorophyll concentration reduces the cold SST bias in the equatorial Pacific (cf. Fig. 3c, d). This bias correction, however, turned out to be ineffective to reduce the warm SST bias in the off-equatorial Pacific. The impact of chlorophyll bias to SST in ESM_on is estimated by comparing the mean states of chlorophyll and SST between the two runs (i.e. subtracting ESM_off from ESM_on). We found that the 0.33 mg/m^3 of annual mean bias of chlorophyll corresponds to the -0.45 °C of annual mean SST cooling in NINO3 region (150°W–90°W, 5°N–5°S).

The vertical structures of biological and physical variables simulated by ESM_on and ESM_off are compared to understand how the chlorophyll difference is linked to the SST change (Fig. 4). The maximum difference of the chlorophyll is 0.5 mg/m^3 which appears in the eastern Pacific at 30 m depth (Fig. 4a). This large surface chlorophyll absorbs the oceanic solar radiation; thereby the shortwave heating is enhanced in the surface layer. In the subsurface ocean, the amount of penetrating solar radiation is reduced because the shortwave energy is already absorbed in the surface layer (i.e., self-shading effect). Thus, this vertical redistribution of oceanic heating leads to more shortwave heating in the surface layer and shortwave cooling in the subsurface ocean (Fig. 4b). This enhances vertical stability in the ocean, and consequently the mixed layer depth (MLD) becomes shallower. Note that the relatively shallower MLD in the equatorial Pacific can induce an enhanced meridional Ekman transport at a given wind forcing (Sweeney et al. 2005), and thus induce excessive equatorial upwelling and shoaling thermocline depth (Fig. 4c). These oceanic changes finally induce the colder SST in the eastern tropical Pacific.

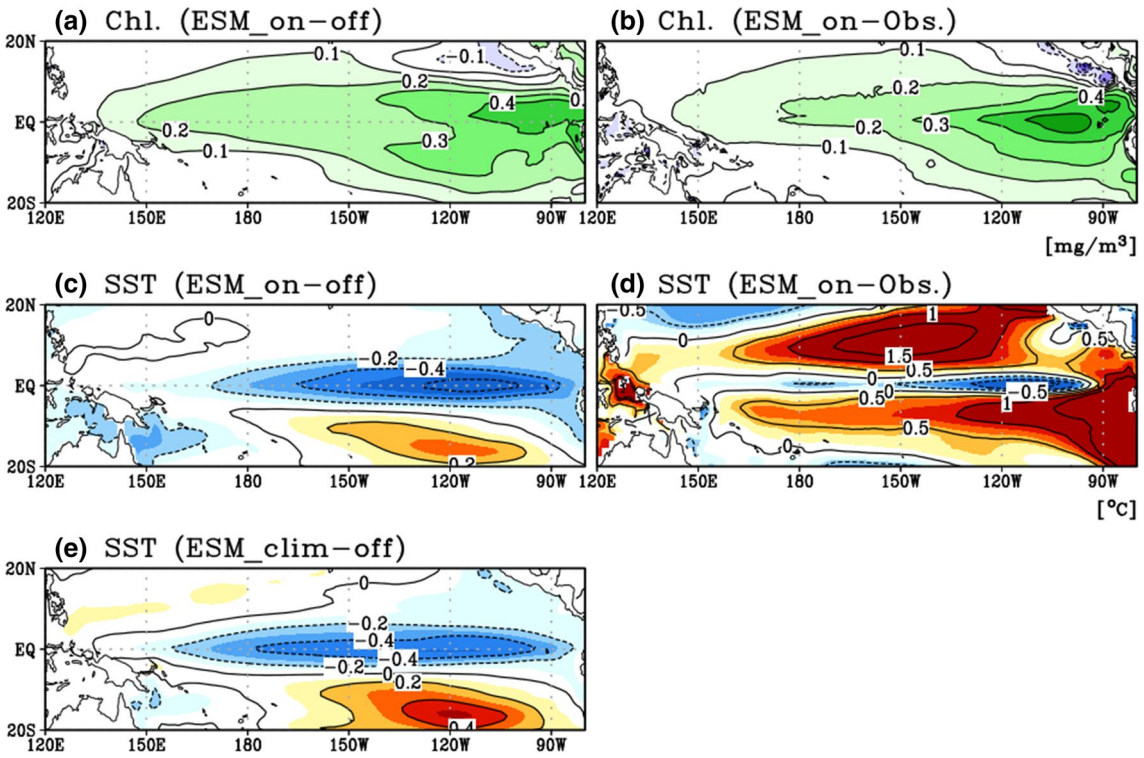

Fig. 3 Mean chlorophyll difference between **a** ESM_on and ESM_off, **b** ESM_on and observation. **c, d** are the same as **a** and **b**, except for sea surface temperature

The magnitudes of SST and zonal wind biases are compared. It is found that the equatorial cold SST bias found in ESM_on is largely affected by chlorophyll bias (Fig. 5a). The initial biologically-induced cooling in the equatorial Pacific can be enhanced by positive Bjerknes feedback. That is, the strong zonal wind bias can be further enhanced by biologically-induced cooling although the magnitude of biologically-induced zonal wind stress is weaker than the intrinsic bias of zonal wind stress (i.e., ESM_on minus observation in Fig. 5b). Accordingly, the precipitation response induced by chlorophyll difference is reduced about 1 mm/day along the equatorial central Pacific due to suppressed convection activities (not shown). One thing to note here is that although correcting chlorophyll bias in ESM_off substantially reduces the equatorial SST bias, wind bias still remains in ESM_off, indicating a weak direct linkage between SST and wind biases along the equator.

3.3 Seasonal dependency of biologically-induced climate response

In general, while equatorial regions are mainly controlled by semi-annual cycle of solar radiation, the cold tongue SST in the equatorial eastern Pacific exhibits a strong annual cycle compared with the western Pacific warm pool SST (Mitchell and Wallace 1992). This zonally asymmetric monthly SST change induces the discrepancy of air–sea coupling strength along the seasonal cycle (Xie and Philander 1994). It is shown in the previous subsection that the biologically-induced SST response can be intensified by air–sea interactions. Therefore, the physical response to the chlorophyll bias may strongly depend on seasonal evolution.

Figure 6 shows the difference between two experiments, ESM_on and ESM_off. Overall chlorophyll difference shows the positive anomalies throughout the year (Fig. 6a) and this positive chlorophyll anomalies can continuously lead to cold responses in the eastern Pacific (Fig. 6d). The biologically-induced cooling reduces precipitation mainly in the central Pacific (Fig. 6c), which is related to the easterly wind difference to the west of the dateline and the westerly wind difference in the eastern Pacific (Fig. 6b). The thermocline depth becomes shoaling due to the enhanced meridional Ekman transport and easterly wind anomalies (Fig. 6e). The overall responses of atmospheric and oceanic variables to the chlorophyll bias can be understood in terms of the air–sea interaction, but with strong seasonality.

Although the chlorophyll bias is slightly larger in May and June, its seasonal difference is not much larger than annual mean difference (Fig. 6a). In contrast, physical responses to the chlorophyll bias show a strong seasonal dependency and their seasonal distributions are somewhat different from that of the chlorophyll bias (cf. Fig. 6a, b–e).

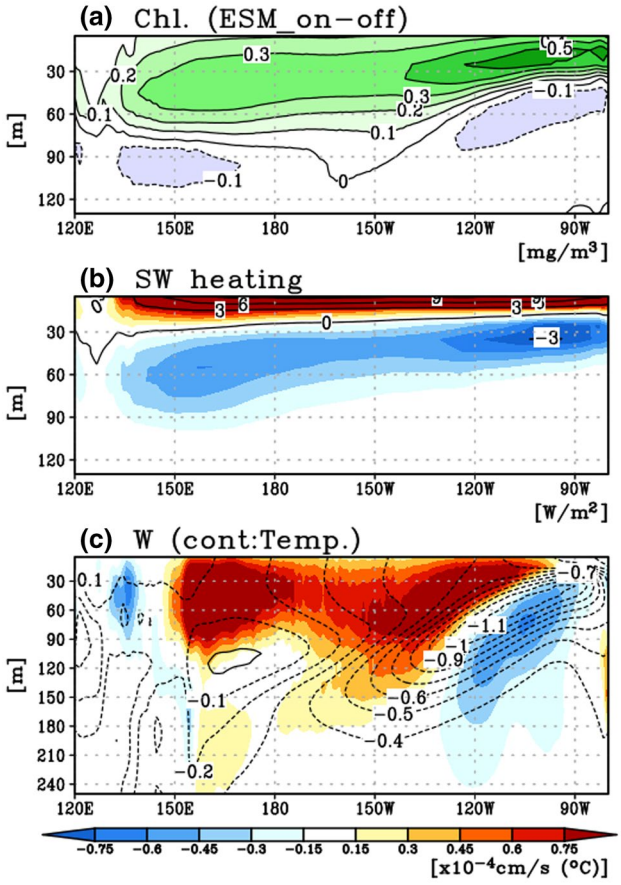

Fig. 4 Mean difference of **a** chlorophyll, **b** shortwave heating, and **c** vertical velocity (shade) and temperature (contour) between ESM_on and ESM_off along the equator (5°N–5°S for chlorophyll and shortwave heating, 2°N–2°S for vertical velocity)

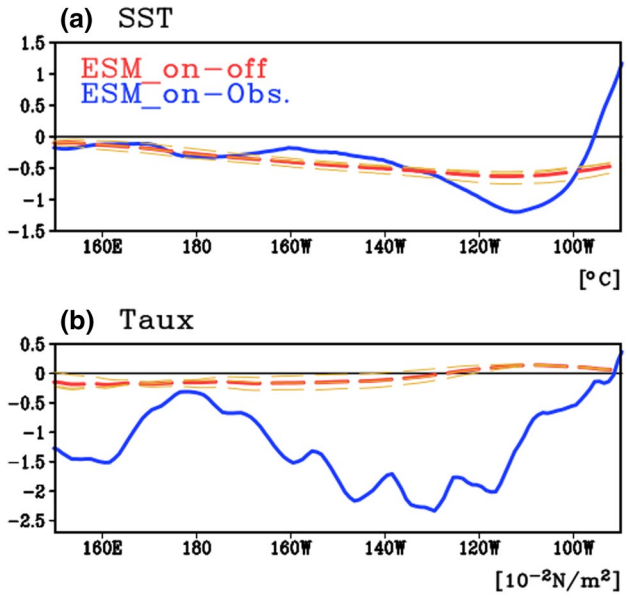

Fig. 5 Mean difference of **a** sea surface temperature, and **b** zonal wind stress between ESM_on and ESM_off (dashed red line) with three ensembles (dashed orange), and between ESM_on and observation (solid blue line) along the equator (2°N–2°S)

For example, the precipitation responses are quite weak during boreal autumn and relatively strong during boreal spring (Fig. 6c). The negative precipitation response (−0.82 mm/day) during April is three times bigger than that (−0.23 mm/day) during September over the central–eastern Pacific (170°E–90°W, 5°S–5°N). The seasonal responses of wind stress to the west of the dateline are consistent with that of the precipitation to some extent. Interestingly, the SST cooling is the strongest in boreal summer. This SST distribution does not match with the precipitation responses although the precipitation is expected to be a direct response to SST forcing. These seasonal dependencies are closely related to the strong seasonal cycle over the tropical Pacific (as shown by contours in Fig. 6c, d). During late boreal summer and autumn, the eastern Pacific exhibits dry and cold states, which are resulted from air–sea coupling processes (Xie and Philander 1994).

These cold and dry conditions affect the atmospheric responses to the biologicallyinduced SST forcing by controlling the strength of air-sea coupling. To examine this point, we calculate the strength of air–sea coupling at each month (Fig. 7). This coupling strength is roughly measured by linear regression coefficients of zonal wind stress and precipitation averaged in central equatorial Pacific (150°E–120°W, 5°N–5°S) against with NINO3.4 SST index (170°W–120°W, 5°N–5°S). The wind stress change associated with the NINO3.4 SST shows positive, indicating that sea surface warming is linked to westerly zonal wind stress (Fig. 7a). Accordingly, the precipitation change associated with NINO3.4 SST also shows overall positive, indicating that the sea surface warming is linked to the precipitation increase (Fig. 7b). Interestingly, both coupling strengths show strong seasonal dependencies. The minimum regression coefficients appear during August and September. This indicates that the responses of the wind stress and precipitation to the same magnitude of SST forcing are weakest in this season. Therefore, in this season, the biologically-induced SST response can be weaker even if the oceanic biogeophysical effect produces the same oceanic temperature response. This seasonal dependency of atmospheric responses can be understood from the background mean states. In August and September, the eastern Pacific is too dry and having strong sinking motion so that the anomalous convective activity is hardly induced even though a considerable SST anomaly exists as many previous studies pointed out (Xie and Philander 1994; Ham and Kug 2011; Kim et al. 2011). In the other seasons, on the other hand, the background mean states are relatively warm and wet, so small SST forcing can easily trigger atmospheric responses.

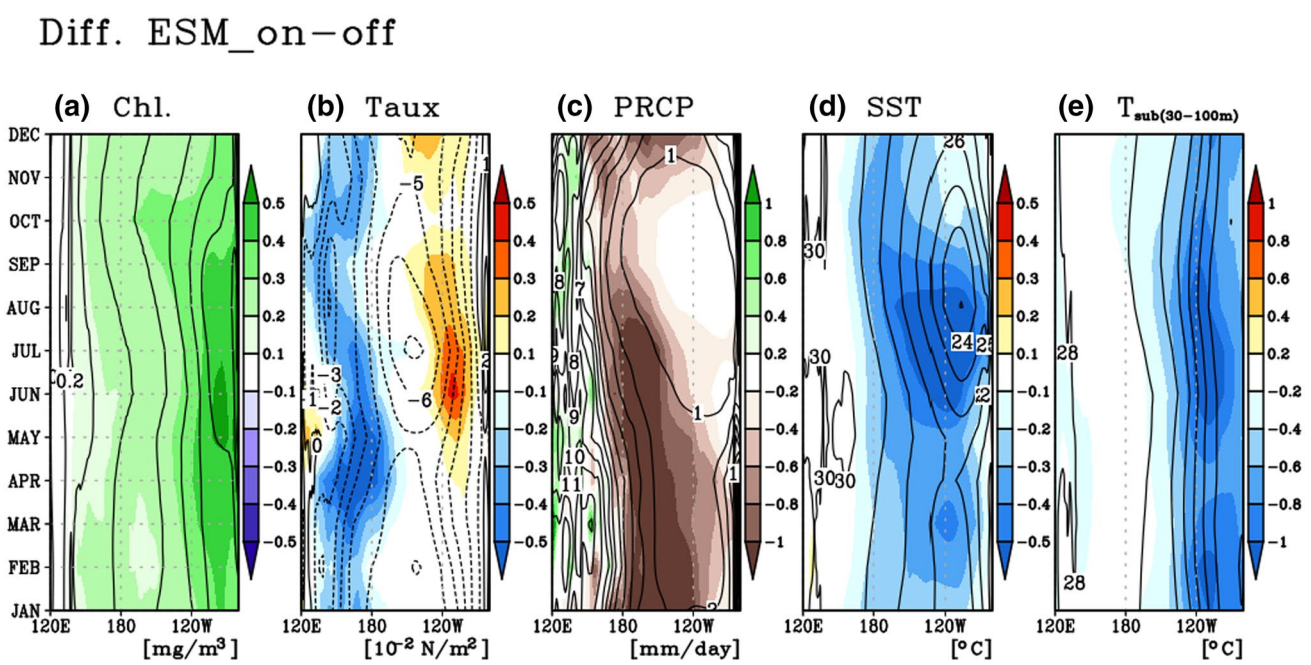

Fig. 6 Climatological monthly mean (contour) and monthly mean difference of **a** chlorophyll, **b** zonal wind stress, **c** precipitation, **d** sea surface temperature, and **e** subsurface temperature averaged in 30–100 m depth between ESM_on and ESM_off (shade) at the equator

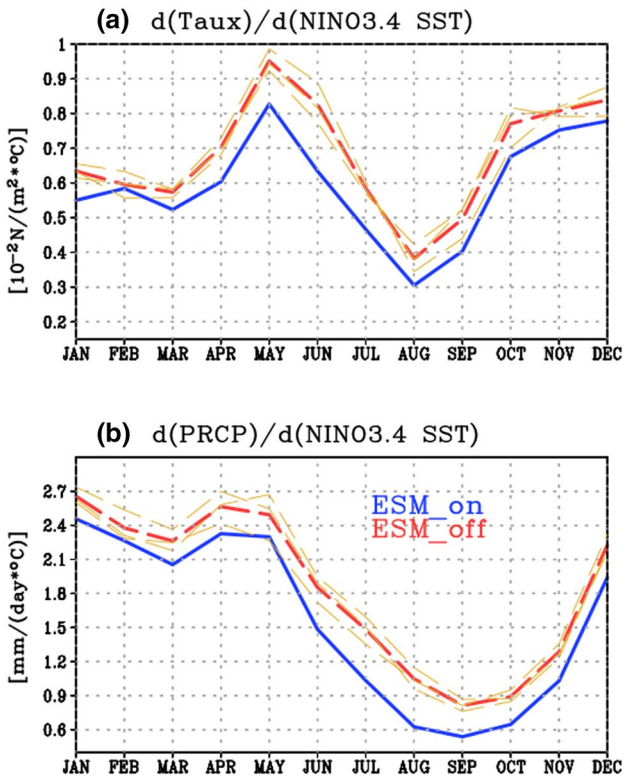

Fig. 7 Regression coefficient of monthly mean **a** zonal wind stress and **b** precipitation anomalies along the central equatorial Pacific (150°E–120°W, 5°N–5°S) against with NINO3.4 sea surface temperature anomalies in ESM_on (blue), three individual ensembles of ESM_off (dashed orange), and ensemble mean of ESM_off (dashed red)

The SST response to the chlorophyll bias is the strongest during boreal summer (Fig. 6d) when the air–sea coupling is suddenly suppressed (Fig. 7a). The negative summertime SST anomaly may be resulted from the shoaling of thermocline in the eastern Pacific (Fig. 6e), which is induced by accumulated upwelling Kelvin waves in response to easterly wind stress forcing. Given that the easterly wind stress is suddenly weakened in the early summer, the thermocline response can be stronger during late summer, which may result in the largest SST changes (Fig. 6d).

Another interesting feature here is that all of the regression coefficients of ESM_on are smaller than ESM_off (Fig. 7). In other words, the coupling strengths are generally stronger in ESM_off than ESM_on. For example, the annual mean regression coefficient for wind stress is increase about 15% from 0.59×10^{-2} N/(m^2 °C) in ESM_on to 0.68×10^{-2} N/(m^2 °C) in ESM_off. The coupling strengths for the precipitation also show similar results. This can be explained by the difference in climatological background mean state. As shown in Fig. 6d, ESM_off simulates the warmer surface ocean than ESM_on, which provides a favorable condition for a stronger atmosphere–ocean coupling strength.

3.4 Response of annual cycle

So far, we have shown that the correction of the chlorophyll bias in the tropical Pacific can reduce the bias in the physical fields of ESM_on and the atmospheric and oceanic

responses to the chlorophyll bias correction show a strong seasonal dependency. The seasonally dependent SST responses may also affect the annual cycle of SST, thus the annual cycle bias in the model can be potentially improved. In this subsection, we examine the improvement of annual cycle in ESM_off compared to ESM_on.

Here, the annual cycle is defined by subtracting the annual mean value of chlorophyll and SST (Fig. 8). The annual cycle of observed chlorophyll shows two peaks (Fig. 8a, contour) due to two peaks of nutrient supply in mixed layer (Strutton et al. 2008). Compared to the observational distribution, ESM_on simulates too high chlorophyll concentration for the August peak, but underestimates the peak in March (Fig. 8a, shading). In fact, the model tends to simulate only one peak of chlorophyll annual cycle, and fails in simulating the peak in March. The annual cycle of zonal wind stress of CM2.1 shows a stronger easterly in August and a weaker westerly in March than the observation (Wittenberg et al. 2006). This makes the stronger annual cycle of MLD in August, which is a cause of the overestimated chlorophyll. In addition, the underestimation of springtime easterly wind and Equatorial Undercurrent (Wittenberg et al. 2006), which is also an important factor for the nutrient supply in the central and eastern Pacific (Strutton et al. 2008), can induce the low chlorophyll in spring.

The annual cycle difference in the equatorial chlorophyll between ESM_on and ESM_off shows a quite similar pattern to that of the chlorophyll bias (cf. Fig. 8a, b). The pattern correlation coefficient between Fig. 8a, b is 0.74, indicating that the ESM_off simulates the better annual cycle of chlorophyll. Therefore, the overestimation of the August peak is much attenuated in the ESM_off simulation. However, the improvement is quite limited for the peak in March although the observed wind stress is prescribed. In this season, the annual cycle of westerly wind in OGCM is enhanced. It means that the annual mean of equatorial easterly wind in OGCM is reduced. This reduces the oceanic mixing and enhances the nutrient limiting condition in March. Therefore, annual cycle of chlorophyll double peak is not completely explained by surface wind driven circulation. Nevertheless, there still has a potential to correct the annual cycle of SST in the eastern Pacific.

The eastern Pacific SST shows the clear single annual cycle in the observation that is highest during March and lowest during September (Fig. 8c). The ESM_on experiment tends to represent the observed annual cycle to some extent, but it simulates the warmer winter and colder spring and summer (Fig. 8c), indicating a shift of the annual cycle. This might be related to the lowest peak in September which locates too far west and terminates about two months earlier compared to the observation (Wittenberg et al. 2006). In particular, the cold bias is much stronger during late summer, indicating the stronger annual cycle in ESM_on. Figure 8d shows the difference between ESM_on and ESM_off, representing chlorophyll bias-induced response. It shows the strong negative SST in late summer, and overall positive

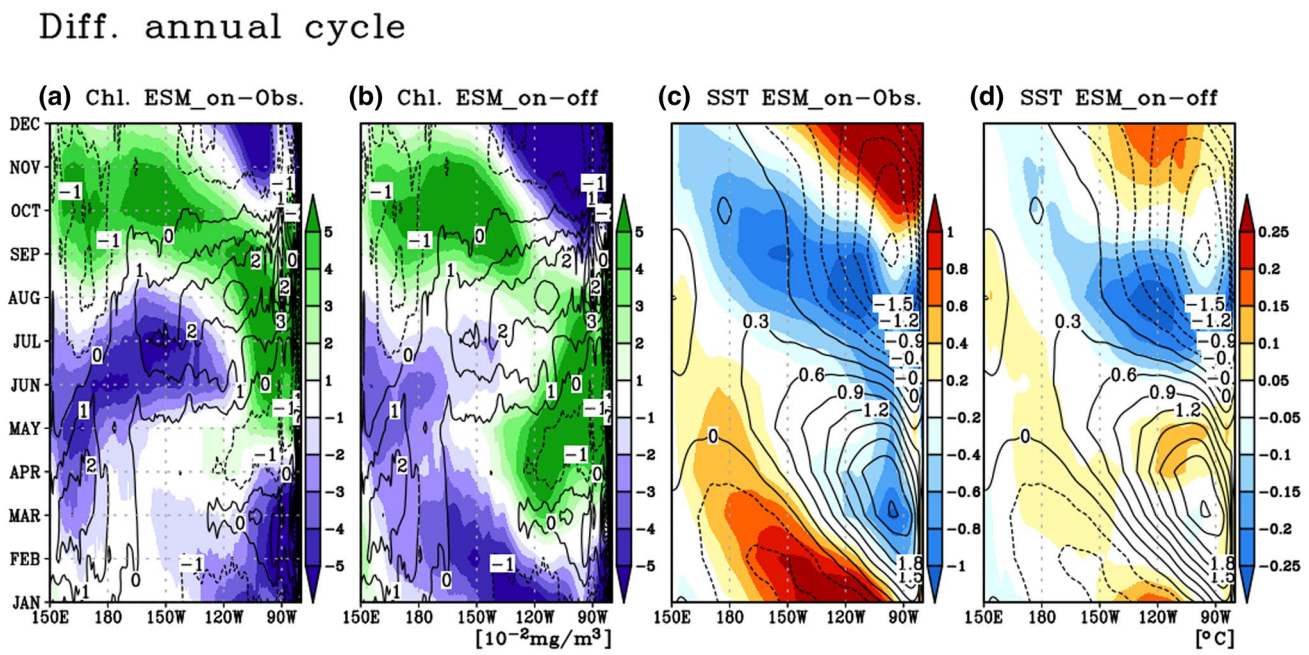

Fig. 8 The differences in annual cycle of **a** chlorophyll between ESM_on and observation, **b** ESM_on and ESM_off after subtracting annual mean values (shade) averaged along the equator (5°N:5°S). **c, d** are the same as **a** and **b**, except for sea surface temperature. Annual cycle of observation is shown as contour

anomalies in winter (Fig. 8d). This indicates that the strong cold bias of ESM_on can be partly explained by the chlorophyll bias in late summer. Although the amplitudes of the SST difference shown in Fig. 8c, d are considerably different, the overall pattern of the difference is fairly similar, implying that the annual cycle of the equatorial SST can be improved by reducing the chlorophyll bias.

To see a clear improvement, the biases of the annual cycle of NINO3 SST in ESM_on and ESM_off are shown in Fig. 9. The annual cycle bias of SST can be partially explained by the annual cycle bias of chlorophyll. Particularly, in August, the most effective season of annual cycle improvement, the SST bias is attenuated by about 25% from −0.97 °C in ESM_on to −0.74 °C in ESM_off. In addition, the annual cycle of SST in the observation has shown the transition between the highest in March and the lowest in September, which corresponds to the transition amplitude of about 2.29 °C (Fig. 8c or d). This transition amplitude in ESM_on turns out to be 2.75 °C in NINO3 region, while that in ESM_off to be 2.63 °C, suggesting that correcting the annual cycle bias of chlorophyll can improve the transition amplitude bias of NINO3 SST from 0.46 to 0.35 °C.

4 Summary and discussion

Nowadays many climate modeling groups continuously develop and improve marine ecosystem processes in their ESMs. Thus, ESMs now have the capability of simulating climate with interactive biogeochemical processes (Taylor et al. 2012). Given that the biological feedback included in ESMs has been recognized to give significant impacts on physical climate systems, the potential effect of chlorophyll bias in the current model should be assessed in the aspect of developing the model.

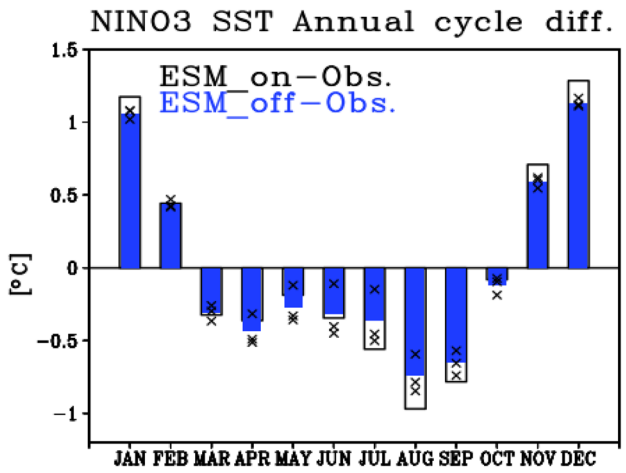

Fig. 9 The differences in annual cycle of NINO3 SST between ESM_on and observation (black bar), and between ESM_on and ESM_off ensemble mean (blue bar) with individual ensemble (cross). The annual cycle is defined as monthly mean anomalies after subtraction of annual mean value

By correcting the tropical Pacific chlorophyll bias in GFDL-ESM, this single model study quantified the impact of chlorophyll bias on the tropical Pacific SST in annual and monthly mean time scales including annual cycle changes. Here, we summarize the major findings.

- The cold SST bias in GFDL-ESM can be partly explained by the chlorophyll bias in the equatorial Pacific. The chlorophyll bias induces an equatorial SST cooling through the biogeophysical feedback processes. The overestimated chlorophyll causes the shallower MLD, equatorial Pacific divergence, shoaling thermocline depth, and intensified upwelling in the equatorial eastern Pacific. Eventually, this leads to cold SST anomalies in the equatorial eastern Pacific. In addition to the oceanic process, the atmospheric positive Bjerknes feedback further enhances the cold SST bias.
- The correction of chlorophyll bias in GFDL-ESM reduces the model's intrinsic cold SST bias in the equatorial Pacific. The impact of chlorophyll bias exhibits strong seasonal dependency due to the seasonality of air-sea coupling strength in the tropical Pacific.
- The chlorophyll bias can also affect the annual cycle of equatorial SST. It is estimated that up to 25% of the SST bias in annual cycle can be explained by the chlorophyll bias.

The chlorophyll and its bias in the ESM can also influence SST variability in the tropical Pacific (Yeh et al. 2014). The cold SST bias weakens the atmospheric feedback process, which in turn affects El Niño-Southern Oscillation (ENSO) variability. Our modeling result shows that the sensitivity of atmospheric responses against with ENSO is increased by the correction of chlorophyll bias in ESM_off. Thus, the strong atmosphere–ocean coupling can enhance ENSO variability compared to the run with the overestimated chlorophyll bias (i.e., ESM_on). In fact, correcting chlorophyll bias amplifies 20% of standard deviation of NINO3 index (averaged from December to February) from 1.14 in ESM_on to 1.40 in ESM_off. The increasing ENSO variability can be explained by the enhanced coupling strength (Fig. 8) due to the reduction of the cold SST bias in the equatorial Pacific. It is noteworthy that ESM_off experiment does not consider the interactive BGC feedback by year-to-year varying chlorophyll, which is acknowledged to damp ENSO variability as highlighted in previous studies (Timmermann and Jin 2002; Jochum et al. 2010; Park et al. 2014a).

While this study is the first experimental study designed to examine the potential relationship between the biases in biological and physical fields, there are still some caveats to

consider. First, the interaction between SST and chlorophyll biases found in GFDL-ESM may not be directly applied to other CMIP5 ESMs. The scatter plot of mean chlorophyll versus mean SST in the eastern equatorial Pacific across 13 CMIP5 ESMs shows a slight negative correlation between the two variables (Fig. 10). The models that simulate colder equatorial Pacific SSTs tend to have higher mean chlorophyll concentration, with a large diversity of chlorophyll concentration in the models simulating cold SSTs. Although this result implies that the potential relationship between the SST and chlorophyll biases seems to be present in different ESMs, the details of the modelling in different model pose a strong limitation to interpret the result. Some models (e.g. HadGEM2-ES(CC), MIROC-ESM, MRI-ESM, MPI-ESM, and CNRM-CM5) either do not include the bio-geophysical feedback process in their models or turn off the bio-geophysical feedback for their CMIP5 runs, although they do have marine ecosystem representation. Therefore, generalizing our results to other model cases should be strongly tempered with caution.

Another caveat of this study is that the impact of chlorophyll bias is examined using a single ESM with a single parameterization of shortwave penetration scheme (Manizza et al. 2005; Griffies 2012). The biogeophysical feedbacks of some CMIP5 ESMs, considering interactive shortwave penetration parameterization by several biogeophysical schemes (Morel 1988; Manizza et al. 2005; Marzeion et al. 2005; Lengaigne et al. 2007; Vichi et al. 2007), are controversial in

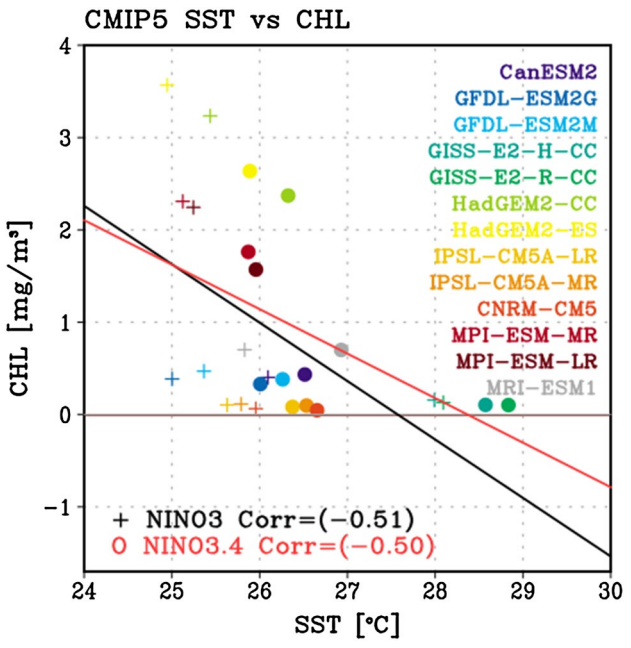

Fig. 10 Scatter plots of climatological mean chlorophyll against mean sea surface temperature simulated from the historical runs of CMIP5 ESMs. The climatological mean is based on the period 1998–2004

that some studies either colder SST (Nakamoto et al. 2001; Manizza et al. 2005; Lin et al. 2007, 2011; Anderson et al. 2009; Gnanadesikan and Anderson 2009; Löptien et al. 2009; Jochum et al. 2010; Park et al. 2014a, b) or warmer SST (Murtugudde et al. 2002; Marzeion et al. 2005; Wetzel et al. 2006; Patara et al. 2012) in the tropical Pacific depending on the model. This implies that evaluating the impact of chlorophyll bias and developing a bias correction method should embrace multiple approaches depending on each ESM's formulation.

The primary finding here is that the chlorophyll bias can contribute to the equatorial Pacific cold bias, a long-lasting bias in climate models. This suggests that the current climate bias in ESMs might be improved by the bias correction in the BGC processes. In turn, the BGC bias is mostly generated from the bias of climate mean state in addition to imperfect parameterizations of biogeochemical processes. That is, there are two-way feedbacks between physical and biogeophysical feedback processes. Thus, in practical sense, the two-way feedbacks should be considered together with improving resolution (Griffies et al. 2015) or tuning the ESM (Dufresne et al. 2013; Hourdin et al. 2017). To do so, understating the two-way interactions in both real and model worlds could be the first indispensable step. The present study here suggests a possible modeling approach in understanding the two-way interactions, and it may be applied to other interactions in ESM frameworks.

Acknowledgements This study was supported by the Korea Meteorological Administration Research and Development Program under Grant KMIPA 2015-1041 and National Research Foundation of Korea (NRF-2017R1A2B3011511). H.-G. Lim is supported by Hyundai Motor Chung Mong-Koo Foundation.

References

Anav A, Friedlingstein P, Kidston M, Bopp L, Ciais P, Cox P, Jones C, Jung M, Myneni R, Zhu Z (2013) Evaluating the land and ocean components of the global carbon cycle in the CMIP5 earth system models. J Clim 26:6801–6843

Anderson JL, Balaji V, Broccoli AJ, Cooke WF (2004) The new GFDL global atmosphere and land model AM2-LM2: evaluation with prescribed SST simulations. J Clim 17:4641

Anderson W, Gnanadesikan A, Wittenberg A (2009) Regional impacts of ocean color on tropical Pacific variability. Ocean Sci 5:313

Aumont O, Bopp L (2006) Globalizing results from ocean in situ iron fertilization studies. Glob Biogeochem Cycles. https://doi.org/10.1029/2005GB002591

Azhar MA, Canfield DE, Fennel K, Thamdrup B, Bjerrum CJ (2014) A model-based insight into the coupling of nitrogen and sulfur cycles in a coastal upwelling system. J Geophys Res Biogeosci 119:264–285. https://doi.org/10.1002/2012JG002271

Bjerknes J (1968) Atmospheric teleconnections from the equatorial Pacific. Mon Weather Rev 97:163–172

Buitenhuis ET, Hashioka T, Quéré CL (2013) Combined constraints on global ocean primary production using observations and models.

Glob Biogeochem Cycles 27:847–858. https://doi.org/10.1002/gbc.20074

Chavez F, Strutton P, Friederich G, Feely R, Feldman G, Foley D, McPhaden M (1999) Biological and chemical response of the equatorial Pacific Ocean to the 1997–98 El Niño. Science 286:2126–2131

Collins WJ, Bellouin N, Doutriaux-Boucher M, Gedney N, Halloran P, Hinton T, Hughes J, Jones CD, Joshi M, Liddicoat S, Martin G, O'Connor F, Rae J, Senior C, Sitch S, Totterdell I, Wiltshire A, Woodward S (2011) Development and evaluation of an earth-system model—HadGEM2. Geosci Model Dev 4:1051–1075. https://doi.org/10.5194/gmd-4-1051-2011

Delworth TL, Broccoli AJ, Rosati A, Stouffer RJ, Balaji V, Beesley JA, Cooke WF, Dixon KW, Dunne J, Dunne KA, Durachta JW, Findell KL, Ginoux P, Gnanadesikan A, Gordon CT, Griffies SM, Gudgel R, Harrison MJ, Held IM, Hemler RS, Horowitz LW, Klein SA, Knutson TR, Kushner PJ, Langenhorst AR, Lee H-C, Lin S-J, Lu J, Malyshev SL, Milly PCD, Ramaswamy V, Russell J, Schwarzkopf MD, Shevliakova E, Sirutis JJ, Spelman MJ, Stern WF, Winton M, Wittenberg AT, Wyman B, Zeng F, Zhang R (2006) GFDL's CM2 global coupled climate models. Part I: formulation and simulation characteristics. J Clim 19:643–674. https://doi.org/10.1175/JCLI3629.1

Dufresne J-L, Foujols M-A, Denvil S, Caubel A, Marti O, Aumont O, Balkanski Y, Bekki S, Bellenger H, Benshila R, Bony S, Bopp L, Braconnot P, Brockmann P, Cadule P, Cheruy F, Codron F, Cozic A, Cugnet D, de Noblet N, Duvel J-P, Ethé C, Fairhead L, Fichefet T, Flavoni S, Friedlingstein P, Grandpeix J-Y, Guez L, Guilyardi E, Hauglustaine D, Hourdin F, Idelkadi A, Ghattas J, Joussaume S, Kageyama M, Krinner G, Labetoulle S, Lahellec A, Lefebvre M-P, Lefevre F, Levy C, Li ZX, Lloyd J, Lott F, Madec G, Mancip M, Marchand M, Masson S, Meurdesoif Y, Mignot J, Musat I, Parouty S, Polcher J, Rio C, Schulz M, Swingedouw D, Szopa S, Talandier C, Terray P, Viovy N, Vuichard N (2013) Climate change projections using the IPSL-CM5 earth system model: from CMIP3 to CMIP5. Clim Dyn 40:2123–2165. https://doi.org/10.1007/s00382-012-1636-1

Dunne JP, Armstrong RA, Gnanadesikan A, Sarmiento JL (2005) Empirical and mechanistic models for the particle export ratio. Glob Biogeochem Cycles. https://doi.org/10.1029/2004gb002390

Dunne JP, Sarmiento JL, Gnanadesikan A (2007) A synthesis of global particle export from the surface ocean and cycling through the ocean interior and on the seafloor. Glob Biogeochem Cycles. https://doi.org/10.1029/2006gb002907

Dunne JP, John JG, Adcroft AJ, Griffies SM, Hallberg RW, Shevliakova E, Stouffer RJ, Cooke W, Dunne KA, Harrison MJ, Krasting JP, Malyshev SL, Milly PCD, Phillipps PJ, Sentman LT, Samuels BL, Spelman MJ, Winton M, Wittenberg AT, Zadeh N (2012) GFDL's ESM2 global coupled climate–carbon earth system models. Part I: physical formulation and baseline simulation characteristics. J Clim 25:6646–6665. https://doi.org/10.1175/jcli-d-11-00560.1

Dunne JP, John JG, Shevliakova E, Stouffer RJ, Krasting JP, Malyshev SL, Milly PCD, Sentman LT, Adcroft AJ, Cooke W, Dunne KA, Griffies SM, Hallberg RW, Harrison MJ, Levy H, Wittenberg AT, Phillips PJ, Zadeh N (2013) GFDL's ESM2 global coupled climate–carbon earth system models. Part II: carbon system formulation and baseline simulation characteristics. J Clim 26:2247–2267. https://doi.org/10.1175/jcli-d-12-00150.1

Esaias WE, Abbott MR, Barton I, Brown OB, Campbell JW, Carder KL, Clark DK, Evans RH, Hoge FE, Gordon HR (1998) An overview of MODIS capabilities for ocean science observations. IEEE Trans Geosci Remote Sens 36:1250–1265

Fan S-M, Moxim WJ, Levy H (2006) Aeolian input of bioavailable iron to the ocean. Geophys Res Lett. https://doi.org/10.1029/2005GL024852

Garcia HE, Locarnini RA, Boyer TP, Antonov JI, Baranova OK, Zweng MM, Reagan J, Johnson DR (2014) World Ocean Atlas 2013, Volume 4: Dissolved Inorganic Nutrients (Phosphate, Nitrate, Silicate). In: Levitus S (ed) NOAA Atlas NESDIS, vol 76. U.S. Government Printing Office, Washington, DC, p 25

Geider R, MacIntyre H, Kana T (1997) Dynamic model of phytoplankton growth and acclimation: responses of the balanced growth rate and the chlorophyll a: carbon ratio to light, nutrient-limitation and temperature. Mar Ecol Prog Ser 148:187–200. https://doi.org/10.3354/meps148187

Gnanadesikan A, Anderson WG (2009) Ocean water clarity and the ocean general circulation in a coupled climate model. J Phys Oceanogr 39:314–332

Green PA, Vörösmarty CJ, Meybeck M, Galloway JN, Peterson BJ, Boyer EW (2004) Pre-industrial and contemporary fluxes of nitrogen through rivers: a global assessment based on typology. Biogeochemistry 68:71–105. https://doi.org/10.1023/b:biog.0000025742.82155.92

Griffies SM (2012) Elements of the modular ocean model (MOM). NOAA Geophysical Fluid Dynamics Laboratory, Princeton

Griffies SM, Winton M, Anderson WG, Benson R, Delworth TL, Dufour CO, Dunne JP, Goddard P, Morrison AK, Rosati A, Wittenberg AT, Yin J, Zhang R (2015) Impacts on ocean heat from transient mesoscale eddies in a hierarchy of climate models. J Clim 28:952–977. https://doi.org/10.1175/jcli-d-14-00353.1

Ham Y-G, Kug J-S (2011) How well do current climate models simulate two types of El Nino? Clim Dyn 39:383–398. https://doi.org/10.1007/s00382-011-1157-3

Horowitz LW, Walters S, Mauzerall DL, Emmons LK, Rasch PJ, Granier C, Tie X, Lamarque J-F, Schultz MG, Tyndall GS, Orlando JJ, Brasseur GP (2003) A global simulation of tropospheric ozone and related tracers: description and evaluation of MOZART, version 2. J Geophys Res Atmos. https://doi.org/10.1029/2002JD002853

Hourdin F, Mauritsen T, Gettelman A, Golaz J-C, Balaji V, Duan Q, Folini D, Ji D, Klocke D, Qian Y, Rauser F, Rio C, Tomassini L, Watanabe M, Williamson D (2017) The art and science of climate model tuning. Bull Am Meteorol Soc 98:589–602. https://doi.org/10.1175/bams-d-15-00135.1

Jochum M, Yeager S, Lindsay K, Moore K, Murtugudde R (2010) Quantification of the feedback between phytoplankton and ENSO in the community climate system model. J Clim 23:2916–2925

Kalnay E, Kanamitsu M, Kistler R, Collins W, Deaven D, Gandin L, Iredell M, Saha S, White G, Woollen J (1996) The NCEP/NCAR 40-year reanalysis project. Bull Am Meteorol Soc 77:437–471

Kim D, Jang Y-S, Kim D-H, Kim Y-H, Watanabe M, Jin F-F, Kug J-S (2011) El Niño–Southern Oscillation sensitivity to cumulus entrainment in a coupled general circulation model. J Geophys Res Atmos. https://doi.org/10.1029/2011jd016526

Large W, Yeager S (2004) Diurnal to decadal global forcing for ocean and seaice models: the data sets and climatologies. Technical Report TN-460+STR, NCAR, p 105

Laufkötter C, Vogt M, Gruber N, Aita-Noguchi M, Aumont O, Bopp L, Buitenhuis E, Doney SC, Dunne J, Hashioka T, Hauck J, Hirata T, John J, Le Quéré C, Lima ID, Nakano H, Seferian R, Totterdell I, Vichi M, Völker C (2015) Drivers and uncertainties of future global marine primary production in marine ecosystem models. Biogeosciences 12:6955–6984. https://doi.org/10.5194/bg-12-6955-2015

Lengaigne M, Menkes C, Aumont O, Gorgues T, Bopp L, André J-M, Madec G (2007) Influence of the oceanic biology on the tropical Pacific climate in a coupled general circulation model. Clim Dyn 28:503–516. https://doi.org/10.1007/s00382-006-0200-2

Lin S-J (2004) A "vertically Lagrangian" finite-volume dynamical core for global models. Mon Weather Rev 132:2293–2307

Lin P, Liu H, Zhang X (2007) Sensitivity of the upper ocean temperature and circulation in the equatorial Pacific to solar radiation penetration due to phytoplankton. Adv Atmos Sci 24:765–780

Lin P, Liu H, Yu Y, Zhang X (2011) Response of sea surface temperature to chlorophyll-a concentration in the tropical Pacific: annual mean, seasonal cycle, and interannual variability. Adv Atmos Sci 28:492–510

Löptien U, Eden C, Timmermann A, Dietze H (2009) Effects of biologically induced differential heating in an eddy-permitting coupled ocean-ecosystem model. J Geophys Res. https://doi.org/10.1029/2008jc004936

Manizza M, Le Quéré C, Watson AJ, Buitenhuis ET (2005) Bio-optical feedbacks among phytoplankton, upper ocean physics and sea-ice in a global model. Geophys Res Lett 32:L05603. https://doi.org/10.1029/2004GL020778

Marzeion B, Timmermann A, Murtugudde R, Jin F-F (2005) Biophysical feedbacks in the tropical Pacific. J Clim 18:58–70

McClain CR (1998) Science quality SeaWiFS data for global biosphere research. Sea Technol 39:10–16

Mignot J, Swingedouw D, Deshayes J, Marti O, Talandier C, Séférian R, Lengaigne M, Madec G (2013) On the evolution of the oceanic component of the IPSL climate models from CMIP3 to CMIP5: a mean state comparison. Ocean Model 72:167–184

Mitchell TP, Wallace JM (1992) The annual cycle in equatorial convection and sea surface temperature. J Clim 5:1140–1156. https://doi.org/10.1175/1520-0442(1992)005<1140:TACIEC>2.0.CO;2

Moore JK, Lindsay K, Doney SC, Long MC, Misumi K (2013) Marine ecosystem dynamics and biogeochemical cycling in the community earth system model [CESM1(BGC)]: comparison of the 1990s with the 2090s under the RCP4.5 and RCP8.5 scenarios. J Clim 26:9291–9312. https://doi.org/10.1175/jcli-d-12-00566.1

Morel A (1988) Optical modeling of the upper ocean in relation to its biogenous matter content (case I waters). J Geophys Res 93:749–710

Morel A, Antoine D (1994) Heating rate within the upper ocean in relation to its bio-optical state. J Phys Oceanogr 24:1652–1665

Murray RJ (1996) Explicit generation of orthogonal grids for ocean models. J Comput Phys 126:251–273

Murtugudde R, Beauchamp J, McClain CR, Lewis M, Busalacchi AJ (2002) Effects of penetrative radiation on the upper tropical ocean circulation. J Clim 15:470–486

Nakamoto S, Kumar SP, Oberhuber J, Ishizaka J, Muneyama K, Frouin R (2001) Response of the equatorial Pacific to chlorophyll pigment in a mixed layer isopycnal ocean general circulation model. Geophys Res Lett 28:2021–2024

Oka A, Hasumi H, Obata H, Gamo T, Yamanaka Y (2009) Study on vertical profiles of rare earth elements by using an ocean general circulation model. Glob Biogeochem Cycles. https://doi.org/10.1029/2008GB003353

Park J-Y, Kug J-S, Park Y-G (2014a) An exploratory modeling study on bio-physical processes associated with ENSO. Prog Oceanogr 124:28–41. https://doi.org/10.1016/j.pocean.2014.03.013

Park J-Y, Kug J-S, Seo H, Bader J (2014b) Impact of bio-physical feedbacks on the tropical climate in coupled and uncoupled GCMs. Clim Dyn 43:1811–1827. https://doi.org/10.1007/s00382-013-2009-0

Patara L, Vichi M, Masina S, Fogli PG, Manzini E (2012) Global response to solar radiation absorbed by phytoplankton in a coupled climate model. Clim Dyn 39:1951–1968. https://doi.org/10.1007/s00382-012-1300-9

Popova EE, Yool A, Coward AC, Dupont F, Deal C, Elliott S, Hunke E, Jin M, Steele M, Zhang J (2012) What controls primary production in the Arctic Ocean? Results from an intercomparison of five general circulation models with biogeochemistry. J Geophys Res Oceans 117:C00D12. https://doi.org/10.1029/2011JC007112

Sallée JB, Shuckburgh E, Bruneau N, Meijers A, Bracegirdle T, Wang Z (2013) Assessment of Southern Ocean mixed-layer depths in CMIP5 models: historical bias and forcing response. J Geophys Res Oceans 118:1845–1862

Séférian R, Bopp L, Gehlen M, Orr JC, Ethé C, Cadule P, Aumont O, Salas y Mélia D, Voldoire A, Madec G (2013) Skill assessment of three earth system models with common marine biogeochemistry. Clim Dyn 40:2549–2573. https://doi.org/10.1007/s00382-012-1362-8

Séférian R, Gehlen M, Bopp L, Resplandy L, Orr JC, Marti O, Dunne JP, Christian JR, Doney SC, Ilyina T, Lindsay K, Halloran PR, Heinze C, Segschneider J, Tjiputra J, Aumont O, Romanou A (2016) Inconsistent strategies to spin up models in CMIP5: implications for ocean biogeochemical model performance assessment. Geosci Model Dev 9:1827–1851. https://doi.org/10.5194/gmd-9-1827-2016

Smith TM, Reynolds RW, Peterson TC, Lawrimore J (2008) Improvements to NOAA's historical merged land-ocean surface temperature analysis (1880–2006). J Clim 21:2283–2296

Stock CA, Dunne JP, John JG (2014) Global-scale carbon and energy flows through the marine planktonic food web: an analysis with a coupled physical–biological model. Progr Oceanogr 120:1–28. https://doi.org/10.1016/j.pocean.2013.07.001

Strutton PG, Evans W, Chavez FP (2008) Equatorial Pacific chemical and biological variability, 1997–2003. Glob Biogeochem Cycles. https://doi.org/10.1029/2007GB003045

Sweeney C, Gnanadesikan A, Griffies SM, Harrison MJ, Rosati AJ, Samuels BL (2005) Impacts of shortwave penetration depth on large-scale ocean circulation and heat transport. J Phys Oceanogr 35:1103–1119

Taylor KE, Stouffer RJ, Meehl GA (2012) An overview of CMIP5 and the experiment design. Bull Am Meteorol Soc 93:485–498

Timmermann A, Jin F-F (2002) Phytoplankton influences on tropical climate. Geophys Res Lett 29:19-11–19-14. https://doi.org/10.1029/2002gl015434

Vancoppenolle M, Bopp L, Madec G, Dunne J, Ilyina T, Halloran PR, Steiner N (2013) Future Arctic Ocean primary productivity from CMIP5 simulations: uncertain outcome, but consistent mechanisms. Glob Biogeochem Cycles 27:605–619. https://doi.org/10.1002/gbc.20055

Vichi M, Pinardi N, Masina S (2007) A generalized model of pelagic biogeochemistry for the global ocean ecosystem. Part I: theory. J Mar Syst 64:89–109

Watanabe S, Hajima T, Sudo K, Nagashima T, Takcmura T, Okajima H, Nozawa T, Kawase H, Abe M, Yokohata T (2011) MIROC-ESM 2010: model description and basic results of CMIP 5–20c3m experiments. Geosci Model Dev 4:845–872

Wetzel P, Maier-Reimer E, Botzet M, Jungclaus J, Keenlyside N, Latif M (2006) Effects of ocean biology on the penetrative radiation in a coupled climate model. J Clim 19:3973–3987

Winton M (2000) A reformulated three-layer sea ice model. J Atmos Ocean Technol 17:525–531

Wittenberg AT, Rosati A, Lau N-C, Ploshay JJ (2006) GFDL's CM2 global coupled climate models. Part III: tropical Pacific climate and ENSO. J Clim 19:698–722. https://doi.org/10.1175/JCLI3631.1

Xie S-P, Philander SGH (1994) A coupled ocean–atmosphere model of relevance to the ITCZ in the eastern Pacific. Tellus A 46:340–350. https://doi.org/10.1034/j.1600-0870.1994.t01-1-00001.x

Yeh S-W, Kug J-S, An S-I (2014) Recent progress on two types of El Nino: observations, dynamics, and future changes. Asia-Pac J Atmos Sci 50(1):69–81. https://doi.org/10.1007/s13143-014-0028-3